Particle & Particle Systems Characterization
www.particle-journal.com

Adsorber Particles with Magnetically-Supported Improved Electrochemical Conversion Behavior for Waste Water Treatment Processes

*Michael Schneider, André Tschöpe, Doris Hanselmann, Thomas Ballweg, Carsten Gellermann, Matthias Franzreb, and Karl Mandel**

Micron-sized supraparticles, consisting of a plurality of discrete nano- and microscale functional units, are assembled and fused by means of a droplet extrusion process. By combining nano magnetite, activated carbon, and conductive carbon with a polymeric binder matrix, particles are obtained which unite good magnetic properties, electrical conductivity, and adsorber activity through the high accessible surface area of the incorporated activated carbon of about 570 $m^2 g^{-1}$, thereby enabling a new approach toward sustainable water treatment processes. Due to the interplay of the components, it is possible to adsorb target substances, dissolved in the water which is demonstrated by the adsorption of the model dye methylene blue. A very fast adsorption kinetic and an adsorption capacity of about 400 mg g^{-1} is determined. By using the developed composite particles, it is also possible to electrochemically alter substances flowing through a magnetically-stabilized fluidized-bed reactor by electrochemically charging/discharging, significantly supported by the magnetic field enabling alternatingly optimum mobility/adsorption phases with contact/charging intervals. The electrochemical conversion can be increased up to 151% depending on the applied flow-rate and electrical voltage. By applying an external magnetic field, a further increase of electrochemical conversion of up to 70% can be observed.

1. Introduction

The treatment of water by removing or degrading unwanted substances like dyes,[1–5] drugs,[6–8] or pesticides,[9–11] the desalination[12–16] as well as the hydrolysis,[17–19] to name but a few, always involves interaction of solid interfaces with the liquid. Often, electrochemical processes play a major role and conventionally, solid state materials such as electrodes are brought into contact with the water.[20–23] If instead of bulk materials small particles would be employed, a higher active interface could be provided and a thorough and homogenous distribution over the whole water body would allow for simultaneous addressing of all compartments of the fluid. However, it is a challenge to handle small particles in a fluid. A promising option to cope with this challenge is to employ magnetic particles. In the recent years, it was successfully demonstrated that magnetic particles are suitable carriers for spatially steerable adsorber materials,[24–28] or photocatalysts.[29–32] Typically, the processes involve the dispersion of the particles in the target fluid and the subsequent magnetic collection after the completion of the required task (for instance, adsorption of target substances formerly dissolved in the water). On the other hand, magnetic particles were also reported to be attractive fillers in columns for so-called magnetic fluidized beds, where an imposed upward fluid flow is imposed on the granular solid phase and in which the gravity, holding the granules down, is supported by a magnetic field.[33–35]

State of the art adsorber particles used for water treatment in fluidized beds are in general static elements as opposed to smart, refreshable adsorber elements insofar as they only possess preset chemical properties which are mostly defined by the synthesis conditions and capacities for adsorbing a limited range of substances. As stated in the beginning, many water treatment processes are driven by electrochemical mechanisms, which principally allow for adjusting adsorption, desorption, altering/degradation of adsorbed substances. Electrochemical treatment involves charge transfer between the fluidized bed particles, which need close contact and sufficient contact time.

M. Schneider, D. Hanselmann, T. Ballweg, Dr. C. Gellermann, Dr. K. Mandel
Fraunhofer Institute for Silicate Research ISC
Neunerplatz 2, 97082 Wuerzburg, Germany
E-mail: karl-sebastian.mandel@isc.fraunhofer.de
A. Tschöpe, Prof. M. Franzreb
Institute of Functional Interfaces
Karlsruhe Institute of Technology
Hermann-von-Helmholtz-Platz 1, 76344 Eggenstein-Leopoldshafen
Germany
Dr. K. Mandel
Chair of Chemical Technology of Material Synthesis
University Wuerzburg
Roentgenring 11, 97070 Wuerzburg, Germany
The ORCID identification number(s) for the author(s) of this article can be found under https://doi.org/10.1002/ppsc.201900487.

DOI: 10.1002/ppsc.201900487

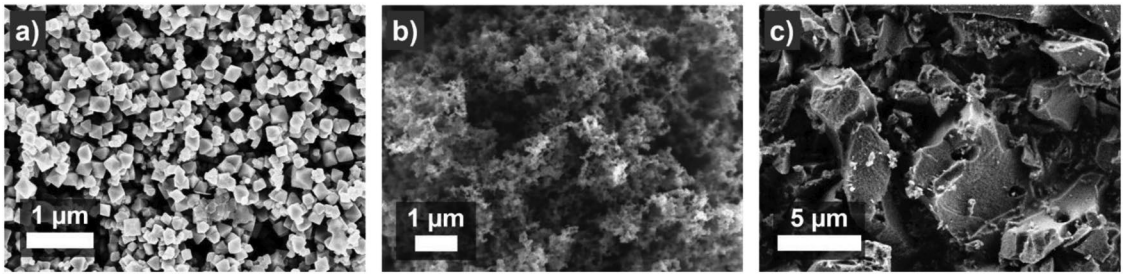

Figure 1. Scanning electron micrograph of the different individual components of the supraparticle: a) magnetic particles, b) conductive carbon, c) activated carbon.

Hence, a toolbox-like synthesis approach where selected materials with special chemical or electrochemical properties can be combined to form one multifunctional particle system to be used in water treatment would be an innovative and promising solution.

By applying magnetic forces on the adsorptive magnetic particles in the fluidized bed, the particles can be arranged and brought into line, resulting in their connection in the fluidized bed. This means that a switchable magnetic property of the particles can be used for optimizing the liquid solid exchange in the flow-through-phase (by low flow resistance and constant mixing with magnetic field being turned off) and the adsorption/desorption/charging interval (by fixing and holding the granules of the fluid bed together with the magnetic field being turned on). In the case of the application of electrochemical conversion, a contact of the particles in the fluidized bed could result in higher conversion rates.[36,37]

Thus, in this work, an attempt was made to create a particle-based system which is electrochemically addressable and thus adjustable and moreover steerable. For this reason, a toolbox-approach was developed which enabled the combination of different functional components in one particle system. Hence, by choosing suitable functional components, the resulting composite particles can be adjusted to the envisaged deployment in water treatment, for example, for enhanced adsorption or for aiding electrochemical decomposition reactions. Herein, an electrically conductive component, a magnetic component, and a component which is very suitable to provide enough surface as adsorber were used. The combination of these three functional constituents results in one single, complex composite particle, a so-called supraparticle,[38] which unites all properties (**Scheme 1**). Due to the toolbox-like character of the supraparticles, such a particle can thus be magnetically steered and electrically addressed, which has great potential to create electrochemically active, magnetic fluidized bed systems of which the proof of principle is reported herein.

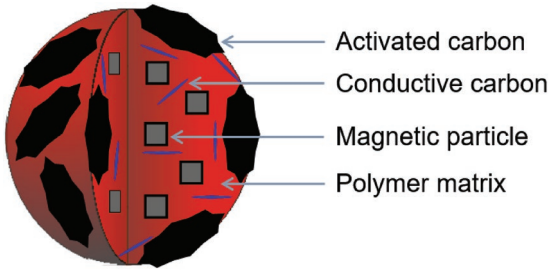

Scheme 1. Schematic depiction of the structure of the developed composite supraparticle.

2. Results and Discussion

2.1. Synthesis and Characterization of Conductive Adsorber Composite Supraparticles

In order to create a particle, which combines magnetic, conductive, and adsorptive properties, ferromagnetic iron oxide (magnetite) nanoparticles, conductive carbon powder (Super C65), and activated carbon particles (Kuraray YP-50F) were selected as the basic building blocks (see **Figure 1**).

To obtain a particle system which unites the three functionalities: magnetic steerability, electrical conductivity, and adsorptive activity, the three functional building blocks need to be combined in an appropriate way. That is, the electrically conductive component must be concentrated and arranged within the particle such that the percolation threshold is overcome. The adsorber building block, that is, herein the activated carbon, must be placed at the surface and very importantly, it must be ensured that the pores are accessible, that is, the activated carbon must form the particle water interface. Finally, the supraparticle must be equipped with a sufficient quantity of magnetic material in order to ensure that the system is still magnetically steerable.

In order to achieve the successful combination of the three building blocks in one particle system, a droplet extrusion process was selected as the method of choice to unite/glue together the three building blocks. With this method, droplets are generated from a vibrating nozzle. The droplets contain the three building blocks, styrene butadiene rubber, and sodium alginate, which are fed into the nozzle. The droplets are subsequently collected in an aqueous solution of $CaCl_2$ leading to the reaction of sodium alginate with $CaCl_2$ and the formation of a stable shell, as depicted in **Figure 2**. The extrusion process itself is further detailed elsewhere.[39] After a subsequent drying procedure, stable and durable particles are obtained.

With this particle formation method, a supraparticle system containing all three functional components could successfully be created (**Figure 3**). As can be seen in the scanning electron microscope (SEM)-images, the resulting supraparticles are not spherical but rather show flattened areas on the surface due

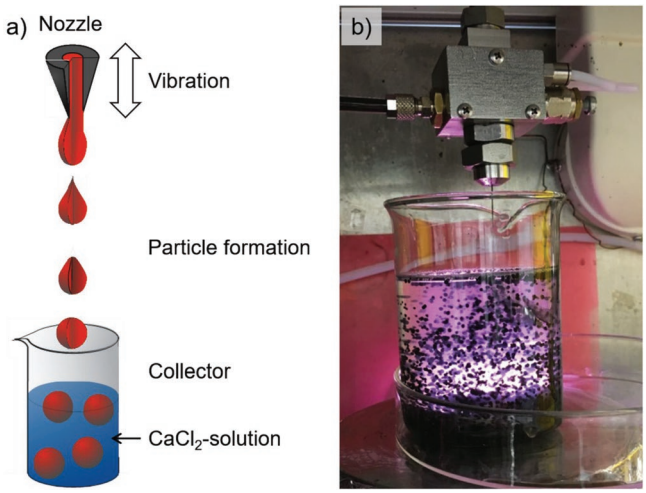

Figure 2. a) Schematic illustration of the formation process of the composite supraparticles including the hardening process in a $CaCl_2$-solution. b) Photograph of the particle formation process.

to the shrinkage that occurs upon drying (see Figure 3a,b). The conductivity of the particle was determined to be about 0.2 S m^{-1}. A closer look at the surface of the supraparticles (see Figure 3c) reveals their composite nature, since different types of primary particles can be seen. Nevertheless, due to their compact and relatively round shape, an application of the particles in a fluidized bed reactor seems realistic.

As mentioned before, the magnetic behavior of the particles plays an important role in the application in a magnetic fluidized bed reactor. Therefore, the magnetic behavior was determined via magnetization measurements and can be seen in Figure 3d. A comparison of the magnetic behavior of the supraparticles with the original magnetite particles shows, that the magnetization drops from 89 emu g^{-1} for pure magnetite to about 21 emu g^{-1} for the supraparticles. Since the magnetization is referred to the mass of the whole particle and magnetite is the only magnetic material used in the synthesis process, one can calculate the actual proportion of magnetite in the supraparticle to be about 24 wt%. This is in good accordance to the initially provided proportion of magnetite for supraparticle formation which was 26 wt%. Therefore, it can be assumed that the particles composition corresponds well with the initially used amounts, as stated in Section 4.

Since the intended use of the developed supraparticles is the adsorption and electrochemical conversion of dissolved substances, the accessible surface area is an important property. Therefore, measurements of the specific surface area via N_2-adsorption and the application of the BET-adsorption model were conducted. The main part of the composite particle providing surface area is the used activated carbon (Kuraray YP-50F) which itself has a specific surface area of 1485 m^2 g^{-1}. The resulting specific surface

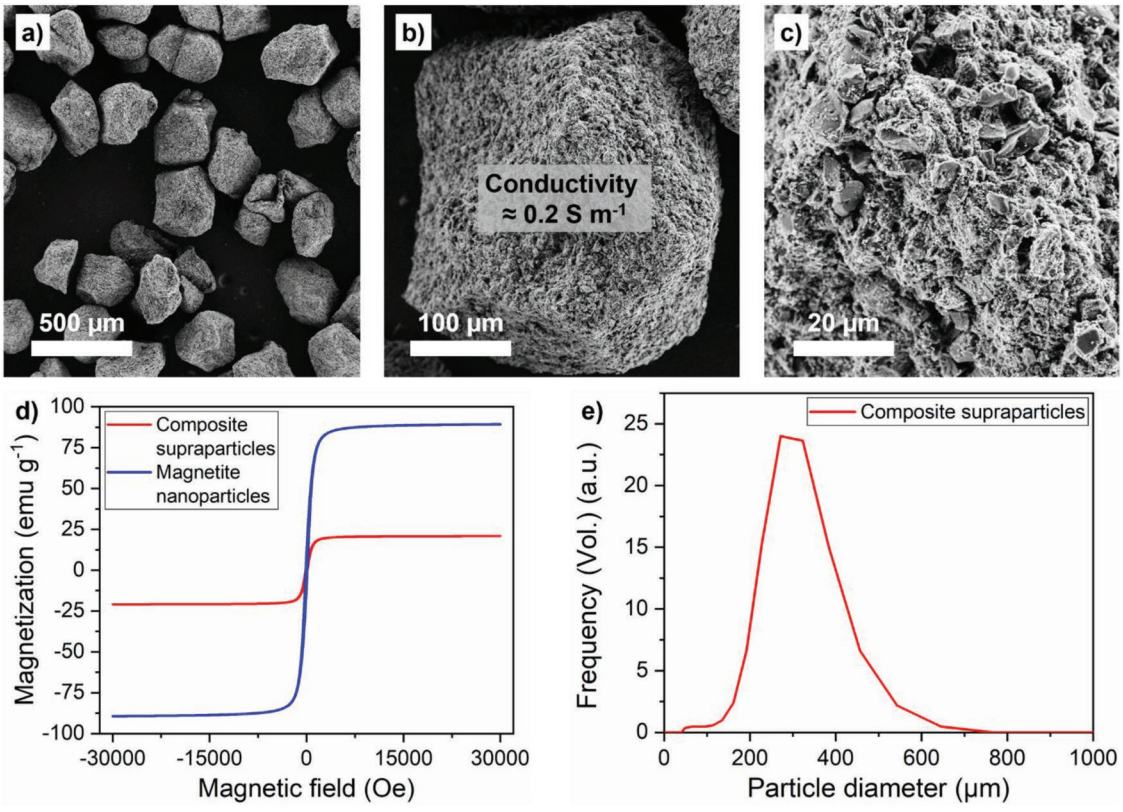

Figure 3. SEM images of the composite particles: a) overview, b) one single particle, c) detailed surface structure. d) Magnetization curves of composite particles compared to the used commercially available magnetite nanoparticles. e) Particle size distribution analyzed by Fraunhofer diffraction measurements of composite particles dispersed in isopropyl alcohol.

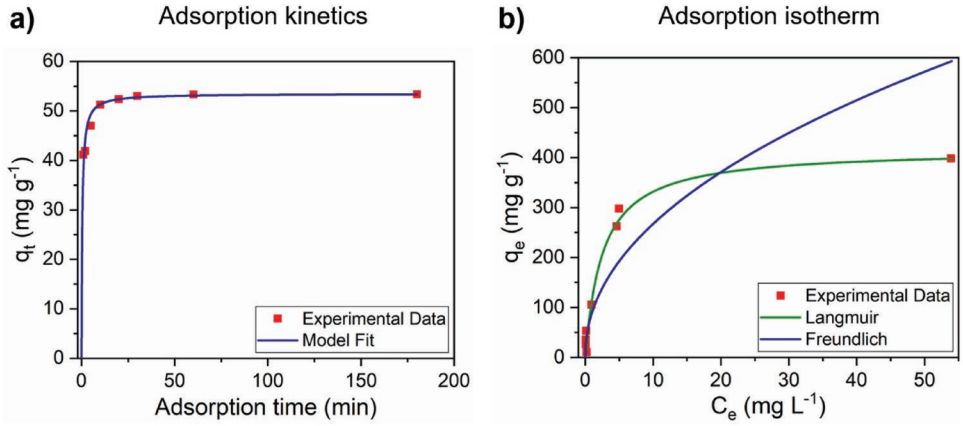

Figure 4. a) Adsorption kinetics of methylene blue on 4.68 g L^{-1} of composite particles at 22 °C. Initial methylene blue concentration = 250 mg L^{-1}, q_t = amount of adsorbed dye in mg per gram of composite particles at a given time. A pseudo-second-order model is fitted to the experimental data set. b) Adsorption isotherm of methylene blue on the composite particles at 22 °C fitted with Langmuir and Freundlich models. q_e = amount of adsorbed dye in mg per gram of composite particles at equilibrium; C_e = concentration of dye in the solution at equilibrium.

area of the composite particles is 567 m^2 g^{-1}. Theoretically, if all the specific surface area of the incorporated activated carbon would be accessible and keeping in mind the proportion of activated carbon in the composite particle, the specific surface area of the composite particles should be about 653 m^2 g^{-1}. Since one cannot assure in the synthesis process that the activated carbon is always located at the surface of the composite supraparticles, the slight reduction of available specific surface area compared to the theoretical value could be expected.

Finally, Fraunhofer diffraction measurements on the dispersed composite supraparticles (Figure 3e) show a broad size distribution with a mean diameter of about 300 µm. In a detailed analysis, the following results for the distribution were calculated: D_{10} = 198 µm, D_{50} = 292 µm, and D_{90} = 414 µm, showing a particle size-range between about 200 µm and about 400 µm.

2.2. Adsorption Properties of Conductive Adsorber Composite Supraparticles

The adsorption behavior of the developed composite supraparticles was investigated at 22 °C. A common approach to investigate the adsorption behavior of materials containing activated carbon is the use of methylene blue (MB) as model organic dye.[1,2,40] As the adsorption behavior of MB is highly sensitive to pH and ionic strength due to its cationic nature[41–43] and due to the well-known possible effects of pH-value and ionic strength on the adsorption behavior of activated carbon,[44–46] the pH-value was fixed to pH 7–8 by using deionized water as described in Section 4. For a later application of the developed supraparticles in waste water, no such adaption of pH value and ionic strength would be possible due to the vast amounts of chemicals that would be necessary. However, due to the toolbox-like character of the supraparticles, an adaption of the chemical and adsorptive properties by changing the employed activated carbon is possible. Both, the adsorption kinetics and the adsorption isotherm of the composite particles were analyzed and are depicted in **Figure 4**.

The purpose of the adsorption kinetics measurements (Figure 4a) was to estimate the time after which the equilibrium was reached. This is absolutely necessary before conducting the experiments for the adsorption isotherm, since there it is crucial to reach equilibrium conditions. As can be seen in Figure 4a, after only 7.5 min, over 95% of the total dye uptake was achieved. Thus, dye uptake was very fast and nearly complete. The experimental data were fitted with both, pseudo-first-order and pseudo-second-order kinetic models, where only the pseudo-second-order model showed good compliance with the data (see **Table 1** for detailed parameters). This adsorption kinetics model is not very informative in terms of mechanisms that occur at the adsorbent–adsorbate interface. Nevertheless, it is very popular in the literature as it provides very satisfactorily fits of adsorption kinetics in the liquid phase.[47]

Finally, also the adsorption isotherm at equilibrium conditions was acquired (Figure 4b). The common Langmuir and Freundlich models (Figure 4b) were used to analyze the experimental data. The generated equation parameters are listed in **Table 2**.

Figure 4b and the values of R^2 in Table 2 indicate, that the Langmuir model fits the isotherm data better than the Freundlich model. This indicates a single layer coverage of the particle surface. Since the Freundlich model should give better fits for porous carbon materials with high surface heterogeneity,[48] it can be assumed that the active sites on the surface all have the same energy, the adsorption is localized, and there is no interaction between adsorbed molecules.

The maximum sorption capacity according to the Langmuir model is about 400 mg of dye per gram of composite

Table 1. Equation parameters of the adsorption kinetics analysis of methylene blue adsorption onto the composite particles at 22 °C.

Pseudo-first-order			Pseudo-second-order		
q_e [mg g^{-1}]	k_1 [min^{-1}]	R^2	q_e [mg g^{-1}]	k_2 [g mg^{-1} min^{-1}]	R^2
7.65	0.854	0.992	53.5	0.0442	0.999

Table 2. Langmuir and Freundlich equation parameters of methylene blue adsorption onto the composite particles at 22 °C.

Langmuir			Freundlich		
q_{max} [mg g^{-1}]	K_L [L mg^{-1}]	R^2	n	K_F [(mg g^{-1}) (mg L^{-1})$^{-n}$]	R^2
417	0.390	0.985	0.473	90.0	0.775

Maximum (monolayer) adsorption capacity q_{max} refers to mg of methylene blue per g of carbon coated particles.

particles. A comparison with other recently published or commercially available magnetic adsorbent materials[43,49] shows that this value is pretty high. The published values range from 15.7 mg g^{-1} for magnetic carbon nanotubes[50] to more than 600 mg g^{-1} for magnetic NP@starch-g-poly(vinyl sulfate)[51] where only very few magnetic materials have monolayer capacities higher than 100 mg g^{-1}. Therefore, our own monolayer capacity of about 400 mg g^{-1} is a very good value. The regeneration of the dye-loaded supraparticles was not investigated in this work, since the focus was to develop a particle system to be employed in a magnetically stabilized fluidized-bed reactor for electrochemical application. However, since the used activated carbon is not altered during the synthesis process of the supraparticles, one can assume, that the regeneration process should be the same as for pure activated carbon materials. In the literature, predominantly regeneration by heating[52–55] is reported.

2.3. Behavior of the Conductive Adsorber Composite Supraparticles in a Magnetically Stabilized Fluidized-Bed Reactor for Electrochemical Application

Having established a multifunctional composite supraparticle with electrical conductivity, magnetic steerability, and accessible activated carbon adsorber surface, the particles were integrated in a magnetically superimposed electrochemical reaction system, to yield a magnetically stabilized fluidized-bed (MSFB) electrode (**Figure 5**). The MSFB reactor for electrochemical applications consists of two separate reaction chambers, the working electrode chamber and the counter electrode chamber. The separation of the two reaction chambers was achieved by means of a cation exchange membrane, which allows the transfer of cations between the two reaction chambers but prevents liquid exchange. The composite particles were used to enlarge the electrode surface in the working electrode chamber. The charge transfer to the composite particles was ensured by means of a fixed platinized titanium electrode. In order to magnetically influence the composite particles in the working electrode chamber, two electric coils were placed around the reaction system. The coils were able to generate a homogeneous magnetic field orientated in flow direction.[34,37]

To demonstrate the proof of principle of the electrochemically addressable, magnetic adsorber particle system, it was studied how well the potassium ferricyanide is reduced to potassium ferrocyanide in the magnetic fluidized bed reactor. For all experiments, a total particle amount of 3 g was used. The results can be seen in **Figure 6**. First, the relative expansion of the fluidized bed with and without the use of an external

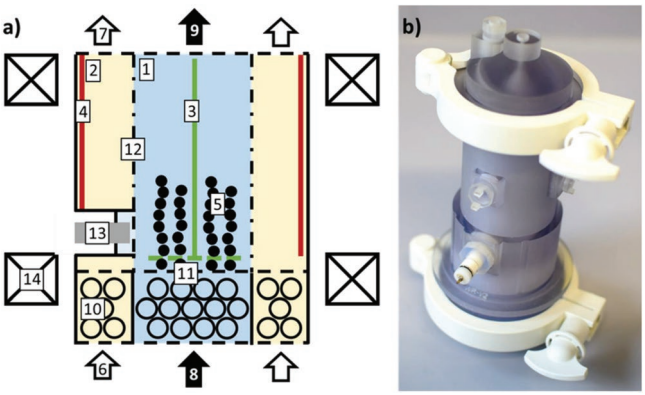

Figure 5. a) Schematic illustration of the electrochemical magnetically stabilized fluidized-bed reactor. In the presence of the external magnetic field, the magnetic composite particles form chains, improving the electrical contact between the particles. 1: working electrode chamber; 2: counter electrode chamber; 3: current source—stationary working electrode; 4: counter electrode; 5: supraparticles; 6: inflow direction of the counter electrode chamber; 7: outflow direction of the counter electrode chamber; 8: inflow direction of the working electrode chamber; 9: outflow direction of the working electrode chamber; 10: glass beads for improved flow distribution; 11: filter for particle retention; 12: ion exchange membrane; 13: reference electrode; 14: electric coil for generating the magnetic field. b) Photograph of the magnetically stabilized fluidized-bed reactor for electrochemical application.

magnetic field at different flow rates was investigated (Figure 6a). Without an external magnetic field, the expansion is slightly larger, and a maximum relative expansion of about 27% could be reached at the highest flow rate of 4 mL min^{-1} compared to about 19% with an external magnetic field of 20 mT. Additionally, the correlation of the expansion to the flow rate seems rather linear. The reduction in expansion, when applying an external magnetic field, can be explained by the tendency of the magnetic particles to form chains along the magnetic field lines, leading to a restricted expansion behavior. For the electrochemical conversion reaction that was investigated, an ordering of the magnetic particles is advantageous due to the better chance of electrical contact between the particles as well as to the current source to charge the electrode particles.

To investigate the particles behavior in the electrochemical conversion of potassium ferricyanide, two similar sets of experiments were conducted (see Figure 6b,c). The flow rate was set to a specific value, namely 2 mL min^{-1} and 4 mL min^{-1} and the conversion was performed at different voltages. Furthermore, the process was conducted using the particles with and without a magnetic field of 20 mT and as reference without the use of the particles. As a measure of the electrochemical conversion, the electric current was analyzed. The results in Figure 6b,c show that without the use of the particles, a variation of the applied voltage has only a minor influence on the electrochemical conversion. Apparently, in this case, the limiting factor of the conversion reaction is not the applied voltage but the electrode area and the mass transfer toward it. An increase in flow rate leads to an improved mass transfer and therefore higher conversion rates indicated by the higher electric current.

For both flow rates, the use of the composite supraparticles as particle electrode in order to enlarge the electrode surface

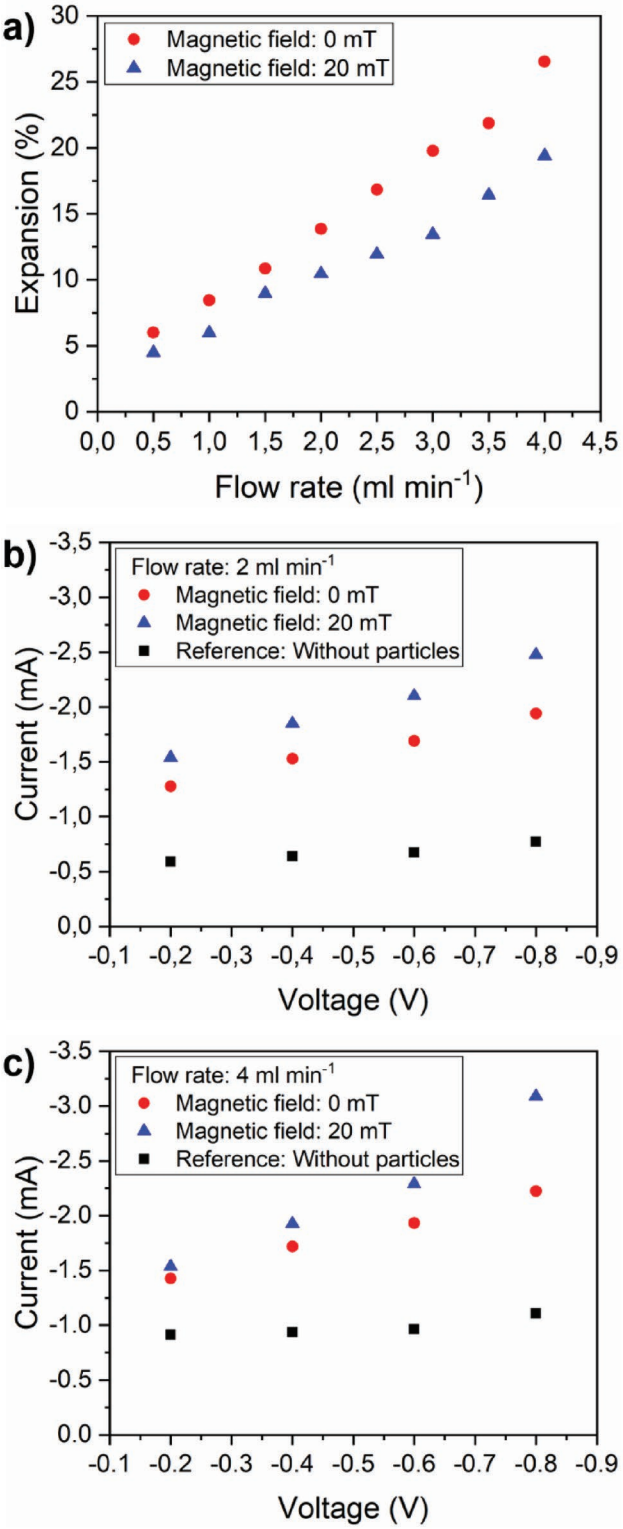

Figure 6. a) Relative expansion of the fluidized composite supraparticles in dependence of the flow rate in mL min^{-1} and of the magnetic field. For all experiments, the particle mass was 3 g. b,c) Electrochemical conversion of potassium ferricyanide at different voltages of –0.2, –0.4, –0.6, and –0.8 V, with and without an external magnetic field of 20 mT and as a reference without composite particles. The measurements were conducted at two different flow rates, namely 2 mL min^{-1} and 4 mL min^{-1}.

leads to a significant increase in the electric current. For a flow rate of 2 mL min^{-1}, the electrochemical conversion is at least doubled for all applied voltages and the increase ranges from 117% for –0.2 V to 151% for –0.8 V. For a flow rate of 4 mL min^{-1}, the increase of electrochemical conversion is smaller (56% for –0.2 V and 100% for –0.8 V), however, the absolute values for the electrical current are higher than for the small flow rate. In addition to that, the electrochemical conversion increases significantly with an increase of applied voltage. Namely, from about –1.3 mA to about –1.9 mA for a flow rate of 2 mL min^{-1} and from about –1.4 mA to about –2.2 mA for a flow rate of 4 mL min^{-1}.

Applying a magnetic field during the experiments leads to a further increase of the electrical current und thus of the electrochemical conversion. At a flow rate of 2 mL min^{-1}, the maximum current of about –1.9 mA at –0.8 V could be increased to about –2.5 mA. At a flow rate of 4 mL min^{-1}, the maximum current of about –2.2 mA at –0.8 V could be increased to about –3.1 mA. As stated, the reason for the magnetic influence onto the achieved electrochemical conversion rates can be explained by an improved conductivity within the particle electrode due to magnetically induced particle chaining.

3. Conclusion

In this work, we developed a composite supraparticle system combining magnetic, sorptive, and electrochemical properties. It was prepared by mixing the three active building blocks magnetic nanoparticles, conductive carbon, and activated carbon with a reactive polymer matrix and processing the mixture with an innovative extrusion process to form spherical composite supraparticles. This particle system is suitable for the adsorption of organic substances from aqueous solutions, which could be shown by the adsorption of the model organic dye methylene blue. Furthermore, the composite supraparticles are suitable for the use in an electrochemical MSFB reactor, using them for increasing the electrode surface. Depending on the applied voltage, flow rate, and external magnetic field, an enhancement of the electrochemical conversion reaction of potassium ferricyanide could be achieved.

4. Experimental Section

Reagents and Materials: Activated carbon "YP-50F" was purchased from Kuraray Europe GmbH. Conductive carbon "Super C65" was purchased from Imerys Graphite & Carbon Switzerland Ltd. Magnetite nanoparticles (diameter 50–100 nm), methylene blue, and calcium chloride dihydrate ($CaCl_2{\cdot}2H_2O$, >99%) were purchased from Sigma-Aldrich. Styrene butadiene rubber (SSBR100, 15% solution in water) was purchased from Targray. Sodium alginate and Tween 80 were purchased from Carl Roth. Potassium ferricyanide trihydrate, potassium ferrocyanide, and potassium chloride were purchased from Merck. All chemicals were used without further purification.

Synthesis of Conductive Adsorber Composite Supraparticles: For the formation of the composite particles, typically, 1 g sodium alginate was dissolved in 40 g water using a Vibramax 100 from Heidolph at 750 rpm. Afterward, 2.0 g of conductive carbon black and 10 g of activated carbon was added and mixed in a Speedmixer DAC400.1 VAC-P from Hauschild for 1 min at 800 rpm and 8 min at 2000 rpm. Then, 6 g of the magnetite particles were added and again mixed in the Speedmixer for 1 min at

800 rpm and 8 min at 2000 rpm. Finally, 6.66 g SSBR100-solution was added and mixed in the Speedmixer for 5 min at 800 rpm. Afterward, the mixture was diluted with 240 g water and 240 g sodium alginate solution (1% in water) and sieved by means of a 45 µm stainless steel sieve to remove larger fragments. The resulting slurry was used to form spherical particles in an innovative new synthesis approach. A detailed explanation of this technique is published elsewhere.[39] In brief, the slurry was extruded through a nozzle. With the nozzle head placed on a tuneable oscillator, a sinusoidal vibration was superimposed to the stream which generates equidistant constrictions leading to the formation of droplets. The formed droplets were collected in a solution of $CaCl_2$ (2%) and Tween80 (0.4%) in water, leading to the reaction of sodium alginate with $CaCl_2$ and the formation of a stable shell. Thereafter, the particles were rinsed with deionized water and ethanol and dried at 60 °C for 2 days and at 107 °C for 3 days.

Adsorption of Methylene Blue on Conductive Adsorber Composite Supraparticles: To determine the adsorption behavior of the developed particles, adsorption tests with methylene blue were carried out, by considering both adsorption kinetics and isotherms. All experiments were carried out at 22 °C in deionized water.

Adsorption Kinetics: For the determination of adsorption kinetics, experiments were carried out with an initial methylene blue concentration of 250 mg L^{-1} and a batch volume of 40 mL. The amount of particles was set to 4.68 g L^{-1} and the adsorption time was varied stepwise from 1 to 180 min. During adsorption, the mixtures were constantly stirred. The solid–liquid separation was performed with a handheld magnet. The remaining amount of dissolved methylene blue was determined by UV–vis spectroscopy. Doing so, the peak intensity in the corresponding absorption spectrum was determined and the residual concentration in water was calculated from a calibration curve. The experimental data were analyzed with pseudo-first-order (Equation (1)) and pseudo-second-order (Equation (2)) kinetic models. The respective equations can be expressed in a linear form as follows

$$\log(q_e - q_t) = \log q_e - \frac{k_1}{2.303} \cdot t \tag{1}$$

$$\frac{t}{q_t} = \frac{1}{k_2 \cdot q_e^2} + \frac{t}{q_e} \tag{2}$$

where the rate constants for the pseudo-first-order and pseudo-second-order kinetic models are k_1 and k_2, respectively. The amounts of methylene blue adsorbed at time t and at equilibrium are q_t and q_e, respectively.

Adsorption Isotherms: The experiments for the determination of the adsorption isotherms were carried out in a similar manner as the kinetics experiments. The initial concentration of methylene blue was kept constant at 250 mg L^{-1}, the batch volume was 40 mL and the concentration of the particles was varied from 0.5 to 23,4 g L^{-1}. During adsorption, the suspensions were stirred at 22 °C until equilibrium was reached. For sampling, the same processes as in the kinetics experiments were conducted. The experimental data were analyzed with Freundlich and Langmuir models. The equations of Freundlich (Equation (3)) and Langmuir (Equation (4)) can be expressed in the following linear form

$$\ln q_e = \ln K_F + n \cdot \ln C_e \tag{3}$$

$$\frac{C_e}{q_e} = \frac{1}{K_L \cdot q_{max}} + \frac{1}{q_{max}} \cdot C_e \tag{4}$$

where the sorption coefficient for Freundlich and Langmuir models are K_F and K_L, respectively. The methylene blue uptake capacity and the concentration of dissolved methylene blue at equilibrium are expressed as q_e and C_e, respectively. The maximum adsorbed amount of methylene blue in a complete monolayer is q_{max}, and n is a constant.

Determination of the Fluidized Bed Expansion: To determine the different expansion states of the fluidized bed at different flow rates and applied magnetic fields, the middle section (working electrode chamber and counter electrode chamber) of the fluidized bed reactor was replaced with a transparent Plexiglas cylinder with the same dimensions as the working electrode chamber. A particle mass of 3 g suspended in water was filled in the fluidized-bed reactor. Afterward, the degree of expansion was determined at flow rate intervals of 0.5 mL min^{-1} in the range from 0.5 to 4 mL min^{-1} with and without the application of an external magnetic field of 20 mT. When a magnetic field was applied, the magnetic field was switched on before the particle fluidization. To determine the percentage of expansion, the height of the fluidized electrode bed and of the initial non-fluidized electrode bed were divided.

Electrochemical Conversion Experiments: A constant flow rate of 2 or 4 mL min^{-1} was applied in the working and counter electrode chamber in the experiments to investigate the electrochemical conversion. It should also be mentioned that different reaction solutions were used for both electrode chambers. In the working electrode chamber, 3 mM potassium ferricyanide was reduced and in the counter electrode chamber 3 mM potassium ferrocyanide was oxidized. 1 M KCl was used as conductive salt for both reaction solutions. Before each experiment, the reaction solutions were gassed with nitrogen and the high electrolyte concentration was used to minimize the oxygen solubility.[56] Between the working and reference electrode, constant voltages of –0.2, –0.4, –0.6, and –0.8 V were applied and the resulting current signal was recorded when a steady-state was reached. In addition, in the experiments with magnetic field influence, a constant magnetic flux density of 20 mT was set.

Analytical Instrumentation: Investigations of the morphology of the material were performed with a SEM using a Zeiss Supra 25 SEM working at 3 keV (field emission). N_2 adsorption studies were carried out using a Micromeritics 3Flex on degassed and dried samples (80 °C, 3×10^{-2} mbar, 24 h) to determine the specific surface area using BET analyses. Magnetic properties of the particles were recorded with a vibrating sample magnetometer (VSM, VersaLabTM 3T, cryogen-free vibrating sample magnetometer), cycling the applied field from –30 to +30 kOe two times with a step rate of 100 Oe s^{-1}. Detailed analyses were carried out by cycling the applied field from –5 to +5 kOe at 5 Oe s^{-1}. The temperature was set to 20 °C. The UV–vis absorption spectra for the determination of dye concentration were measured in the range of 200–800 nm by a spectrometer Specord 50, Analytik Jena AG.

Acknowledgements

This work was supported by the German Federal Ministry of Education and Research (BMBF) under the project ElektroWirbel (FKZ 13XP5008).

Conflict of Interest

The authors declare no conflict of interest.

Keywords

composite supraparticles, dye adsorption, electrochemical conversion, magnetic particles, water purification

Received: December 13, 2019
Revised: December 29, 2019
Published online: January 29, 2020

[1] V. K. Garg, M. Amita, R. Kumar, R. Gupta, *Dyes Pigm.* **2004**, *63*, 243.
[2] W. G. Kuo, *Water Res.* **1992**, *26*, 881.
[3] C.-C. Su, M. Pukdee-Asa, C. Ratanatamskul, M.-C. Lu, *Desalination* **2011**, *278*, 211.

[4] H. Hayat, Q. Mahmood, A. Pervez, Z. A. Bhatti, S. A. Baig, *Sep. Purif. Technol.* **2015**, *154*, 149.
[5] P. Manoj Kumar Reddy, B. Rama Raju, J. Karuppiah, E. Linga Reddy, C. Subrahmanyam, *Chem. Eng. J.* **2013**, *217*, 41.
[6] H. Krause, B. Schweiger, E. Prinz, J. Kim, U. Steinfeld, *J. Electrost.* **2011**, *69*, 333.
[7] M. Magureanu, D. Piroi, N. B. Mandache, V. David, A. Medvedovici, V. I. Parvulescu, *Water Res.* **2010**, *44*, 3445.
[8] M. Magureanu, N. B. Mandache, V. I. Parvulescu, *Water Res.* **2015**, *81*, 124.
[9] H. Bachmann Pinto, B. Miguel de Souza, M. Dezotti, *J. Cleaner Prod.* **2018**, *201*, 1061.
[10] L. Ghimici, I. A. Dinu, *Sep. Purif. Technol.* **2019**, *209*, 698.
[11] N. Wardenier, P. Vanraes, A. Nikiforov, S. W. H. van Hulle, C. Leys, *J. Hazard. Mater.* **2019**, *362*, 238.
[12] D. Cohen-Tanugi, J. C. Grossman, *Nano Lett.* **2012**, *12*, 3602.
[13] T. Humplik, J. Lee, S. C. O'Hern, B. A. Fellman, M. A. Baig, S. F. Hassan, M. A. Atieh, F. Rahman, T. Laoui, R. Karnik, E. N. Wang, *Nanotechnology* **2011**, *22*, 292001.
[14] Y. Oren, *Desalination* **2008**, *228*, 10.
[15] A. Subramani, J. G. Jacangelo, *Water Res.* **2015**, *75*, 164.
[16] J.-B. Lee, K.-K. Park, H.-M. Eum, C.-W. Lee, *Desalination* **2006**, *196*, 125.
[17] D. Lachos-Perez, G. A. Tompsett, P. Guerra, M. T. Timko, M. A. Rostagno, J. Martínez, T. Forster-Carneiro, *Bioresour. Technol.* **2017**, *243*, 1069.
[18] D. Lachos-Perez, F. Martinez-Jimenez, C. A. Rezende, G. Tompsett, M. Timko, T. Forster-Carneiro, *J. Supercrit. Fluids* **2016**, *108*, 69.
[19] J. M. Prado, D. Lachos-Perez, T. Forster-Carneiro, M. A. Rostagno, *Food Bioprod. Process.* **2016**, *98*, 95.
[20] C. Comninellis, *Electrochim. Acta* **1994**, *39*, 1857.
[21] C. A. Martínez-Huitle, M. Panizza, *Curr. Opin. Electrochem.* **2018**, *11*, 62.
[22] S. Stucki, R. Koetz, B. Carcer, W. Suter, *J. Appl. Electrochem.* **1991**, *21*, 99.
[23] P. V. Nidheesh, G. Divyapriya, N. Oturan, C. Trellu, M. A. Oturan, *ChemElectroChem* **2019**, *6*, 2124.
[24] K.-W. Jung, S. Lee, Y. J. Lee, *Bioresour. Technol.* **2017**, *245*, 751.
[25] Y. Zhao, J. Li, L. Zhao, S. Zhang, Y. Huang, X. Wu, X. Wang, *Chem. Eng. J.* **2014**, *235*, 275.
[26] J. Sun, Y. Chen, H. Yu, L. Yan, B. Du, Z. Pei, *J. Colloid Interface Sci.* **2018**, *532*, 474.
[27] M. Schneider, T. Ballweg, L. Groß, C. Gellermann, A. Sanchez-Sanchez, V. Fierro, A. Celzard, K. Mandel, *Part. Part. Syst. Charact.* **2019**, *36*, 1800537.
[28] A. Drenkova-Tuhtan, M. Schneider, M. Franzreb, C. Meyer, C. Gellermann, G. Sextl, K. Mandel, H. Steinmetz, *Water Res.* **2017**, *109*, 77.
[29] S. Shylesh, V. Schünemann, W. R. Thiel, *Angew. Chem., Int. Ed.* **2010**, *49*, 3428.
[30] A.-H. Lu, W. Schmidt, N. Matoussevitch, H. Bönnemann, B. Spliethoff, B. Tesche, E. Bill, W. Kiefer, F. Schüth, *Angew. Chem., Int. Ed.* **2004**, *43*, 4303.
[31] F. Nemati, M. M. Heravi, R. Saeedi Rad, *Chin. J. Catal.* **2012**, *33*, 1825.
[32] A. Pourjavadi, S. H. Hosseini, M. Doulabi, S. M. Fakoorpoor, F. Seidi, *ACS Catal.* **2012**, *2*, 1259.
[33] X.-D. Tong, Y. Sun, *Biotechnol. Prog.* **2003**, *19*, 1721.
[34] J. Hristov, L. Fachikov, *China Particuol.* **2007**, *5*, 11.
[35] I. Pereiro, S. Tabnaoui, M. Fermigier, O. Du Roure, S. Descroix, J.-L. Viovy, L. Malaquin, *Lab Chip* **2017**, *17*, 1603.
[36] J. R. Backhurst, J. M. Coulson, F. Goodridge, R. E. Plimley, M. Fleischmann, *J. Electrochem. Soc.* **1969**, *116*, 1600.
[37] A. Tschöpe, M. Wyrwoll, M. Schneider, K. Mandel, M. Franzreb, *Chem. Eng. J.* **2020**, *385*, 123845.
[38] S. Wintzheimer, T. Granath, M. Oppmann, T. Kister, T. Thai, T. Kraus, N. Vogel, K. Mandel, *ACS Nano* **2018**, *12*, 5093.
[39] T. Ballweg, H. von Daake, D. Hanselmann, D. Stephan, K. Mandel, G. Sextl, *Appl. Mater. Today* **2018**, *11*, 231.
[40] F. Huang, L. Chen, H. Wang, Z. Yan, *Chem. Eng. J.* **2010**, *162*, 250.
[41] Y. Song, Y. Duan, L. Zhou, *J. Colloid Interface Sci.* **2018**, *529*, 139.
[42] G. Gong, F. Zhang, Z. Cheng, L. Zhou, *Int. J. Biol. Macromol.* **2015**, *81*, 205.
[43] Z. Cheng, J. Liao, B. He, F. Zhang, F. Zhang, X. Huang, L. Zhou, *ACS Sustainable Chem. Eng.* **2015**, *3*, 1677.
[44] Y. S. Al-Degs, M. I. El-Barghouthi, A. H. El-Sheikh, G. M. Walker, *Dyes Pigm.* **2008**, *77*, 16.
[45] J.-M. Chern, C.-Y. Wu, *Water Res.* **2001**, *35*, 4159.
[46] J. J. M. Órfao, A. L. M. Silva, J. C. V. Pereira, S. A. Barata, I. M. Fonseca, P. C. C. Faria, M. F. R. Pereira, *J. Colloid Interface Sci.* **2006**, *296*, 480.
[47] V. Fierro, V. Torné-Fernández, D. Montané, A. Celzard, *Microporous Mesoporous Mater.* **2008**, *111*, 276.
[48] P. Girods, A. Dufour, V. Fierro, Y. Rogaume, C. Rogaume, A. Zoulalian, A. Celzard, *J. Hazard. Mater.* **2009**, *166*, 491.
[49] M. Oppmann, M. Wozar, J. Reichstein, K. Mandel, *ChemNanoMat* **2018**, *6*, 141.
[50] J.-L. Gong, B. Wang, G.-M. Zeng, C.-P. Yang, C.-G. Niu, Q.-Y. Niu, W.-J. Zhou, Y. Liang, *J. Hazard. Mater.* **2009**, *164*, 1517.
[51] A. Pourjavadi, A. Abedin-Moghanaki, A. Tavakoli, *RSC Adv.* **2016**, *6*, 38042.
[52] K. Y. Foo, B. H. Hameed, *J. Anal. Appl. Pyrolysis* **2012**, *98*, 123.
[53] G. San Miguel, S. D. Lambert, N. J. D. Graham, *Water Res.* **2001**, *35*, 2740.
[54] D. Xin-hui, C. Srinivasakannan, L. Jin-sheng, *J. Taiwan Inst. Chem. Eng.* **2014**, *45*, 1618.
[55] K. Y. Foo, B. H. Hameed, *Bioresour. Technol.* **2012**, *119*, 234.
[56] R. Battino, T. R. Rettich, T. Tominaga, *J. Phys. Chem. Ref. Data* **1983**, *12*, 163.